Applied Energy 382 (2025) 125216

Contents lists available at ScienceDirect

Applied Energy

journal homepage: www.elsevier.com/locate/apenergy

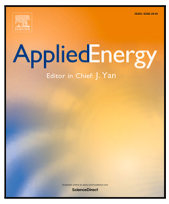

Thermal performance response and heat load redistribution mechanism of a deep U-type borehole heat exchanger in heating systems

Chaofan Chen [a,b,*], Francesco Witte [c], Reza Taherdangkoo [a,b], Wanlong Cai [d,**], Shuang Chen [e], Yanlong Kong [f], Haibing Shao [g], Mathias Hofmann [h], Thomas Nagel [a,b,g]

[a] Geotechnical Institute, Technische Universität Bergakademie Freiberg, 09599 Freiberg, Germany
[b] Freiberg Center for Water Research (ZeWaF), 09599 Freiberg, Germany
[c] Institute of Networked Energy Systems, German Aerospace Center (DLR), 26129 Oldenburg, Germany
[d] School of Human Settlements and Civil Engineering, Xi'an Jiaotong University, 710049, Xi'an, China
[e] Federal Institute for Geosciences and Natural Resource (BGR), 30655 Hannover, Germany
[f] Institute of Geology and Geophysics, Chinese Academy of Sciences, 100029 Beijing, China
[g] Helmholtz Centre for Environmental Research-UFZ, Permoserstraße 15, 04318 Leipzig, Germany
[h] Technische Universität Berlin, Chair of Energy Engineering and Climate Protection, Marchstraße 18, 10587 Berlin, Germany

ARTICLE INFO

Keywords:
Deep U-type borehole heat exchanger (DUBHE)
Ground source heat pump
Building heating
Heat load redistribution
District heating system

ABSTRACT

Deep closed-loop borehole heat exchanger systems have gained significant attention in recent years for extracting geothermal energy to effectively heat buildings, e.g. by integrating them into district heating systems. In this work, a 3D numerical model of the pilot Deep U-type Borehole Heat Exchanger (DUBHE) system that was recently implemented in Xi'an, China, is established based on the OpenGeoSys software. The model is fully validated by 2-months of monitoring data from the pilot project. Then, a thermodynamic heat pump model is further coupled to investigate the transient thermal response of the DUBHE to the heat pump's off-design performance. Subsequently, dynamic operations in a district heating system are simulated to evaluate the flexibility of the DUBHE-couple heat pump system. For the first time, the mechanism of heat load distribution by the heat pump and the behavior of heat load redistribution during operation are clarified between the subsurface DUBHE and the heat pump. The maximum sustainable heating power of the whole system is found to be around 780 kW in 120-day operation with the working fluid R410A and the required feed flow temperature of 65°C in the heat pump. With increasing operation time, the heat load distributed to the DUBHE decreases by more than 21% in 120 days due to the decrease in the heat pump performance. The R600 heat pump has the best performance and efficiency among four different working fluids, but leads to a 3.4°C reduction in the outflow temperature of the DUBHE compared to the R410A heat pump. This over-extracted performance of the DUBHE poses a challenge to its sustainable operation in terms of the circulation fluid temperature of the DUBHE. In the two operation patterns of integrating into the district heating system, the subsurface DUBHE can provide both around 70% of the total heat power to the district heating system. The average annual COP is 0.2 higher with low feed flow temperature to the district heating system and more frequent shutdown operation, showing significant flexibility in integrating the DUBHE-coupled heat pump system into the district heating system.

1. Introduction

Deep geothermal energy has been widely extracted in recent years to supply heat to buildings. In conventional hydrothermal exploitation, a sufficiently permeable reservoir is required to establish an open-loop system in the subsurface. This limits the locations available for the utilization of deep geothermal energy. In comparison, the closed-loop borehole heat exchanger (BHE) system, due to its dependence on location, is attracting more attention in the geothermal heating and cooling industry [1–4]. Conventionally, engineers tend to couple more BHEs in an array to scale up the heat extraction capacity of the closed-loop system from the shallow subsurface [5,6]. Other efforts are focusing on the extension of the heat exchange surface of the

* Corresponding author at: Geotechnical Institute, Technische Universität Bergakademie Freiberg, 09599 Freiberg, Germany.
** Corresponding author.
E-mail addresses: chaofan.chen@ifgt.tu-freiberg.de (C. Chen), wanlongcai@mail.xjtu.edu.cn (W. Cai).

https://doi.org/10.1016/j.apenergy.2024.125216
Received 1 July 2024; Received in revised form 12 August 2024; Accepted 21 December 2024
Available online 1 January 2025

Nomenclature

Roman letters

c	Specific heat capacity ($J\,kg^{-1}\,K^{-1}$)
D_e	Equivalent diameter of the pipe (m)
H	Heat sink/source term ($W\,m^{-3}$)
h	Specific enthalpy of circulation fluid ($J\,kg^{-1}$)
$\mathbf{I}$	Identity tensor (–)
k_s	Roughness of pipe (mm)
L	Length of pipe (m)
$\dot{m}$	Mass flow of circulation fluid ($kg\,s^{-1}$)
P	Power (W)
p	Hydraulic pressure loss in the pipe network (W)
Q	Heat (W)
q_n	Heat flux ($W\,m^{-2}$)
Re	Reynolds number (–)
T	Temperature (°C)
t	Time (s)
$\mathbf{v}$	Vector of flow velocity ($m\,s^{-1}$)
x	Mass fraction of circulation fluid (–)

Greek Letters

α	Thermal diffusivity ($m^2\,h^{-1}$)
β_L	Longitudinal heat dispersivity (m)
Γ	Boundary
λ	Thermal conductivity ($W\,m^{-1}\,K^{-1}$)
Λ	Thermal hydrodynamic dispersion tensor ($W\,m^{-1}\,K^{-1}$)
Φ	Heat transfer coefficient ($W\,m^{-2}\,K^{-1}$)
ρ	Density ($kg\,m^{-3}$)
Θ	Darcy friction factor (–)

Operators

Δ	Difference operator
∇	Nabla vector operator
$\sum$	Integral operator

Subscripts

f	Circulation fluid in borehole
fl	Circulation fluid in pipe network
g	Grout
i	Inner pipe (outflow)
in	Inlet
max	Maximum
o	Outer pipe (inflow)
out	Outlet
s	Soil/rock

Abbreviations

AGS	Advanced Geothermal System
BHE	Borehole Heat Exchanger
COP	Coefficient of Performance
DUBHE	Deep U-type Borehole Heat Exchanger
GSHP	Ground Source Heat Pump
HP	Heat Pump
OGS	OpenGeoSys
TESPy	Thermal Engineering Systems in Python

closed loop with multilateral wells to enhance the system's capacity. For example, Chen et al. [7] proposed a deep U-type borehole heat exchanger (DUBHE) system by connecting two deep boreholes at the bottom. They found that the average coefficient of system performance is 1.7 times higher over a period of 10 heating seasons, considering the electricity consumed by the heat pump's compressor and the circulation pump. Malek et al. [8] analyzed an Advanced Geothermal System (AGS) with four lateral wells for electricity generation and concluded that drilling cost has to be reduced by 50% to enable cost-competitive implementations. Kelly and McDermott [9], Chen and Feng [10], and Chong et al. [11] have evaluated the heat extraction performance of large deep closed-loop systems and quantified the heat production performance of several types of deep closed-loop systems. Regarding the application and optimization of the deep closed-loop DUBHE system in real projects, Jiang et al. [12] evaluated the long-term performance of the DUBHE considering the influence of different geological parameters using the Taguchi method. Xiao et al. [13] used a coupled techno-economic model to analyze the net present value of a U-shaped closed-loop geothermal system in Xi'an, China. Blázquez et al. [14] studied the influence of different grouting materials in vertical geothermal closed-loop systems. Taking into account different working fluids in the closed loops in the subsurface, Sun et al. [15] evaluated the performance of heat production using CO_2 as the circulation fluid. The heat extraction performance of different types of closed-loop system under different construction and operation conditions has been thoroughly studied in the literature. However, since all of the aforementioned studies focused only on the subsurface loop, the thermal response performance of the subsurface closed-loop DUBHE remains unclear when operated in heating systems.

When using a closed-loop geothermal system for space heating, the subsurface loop needs to be coupled with a heat pump to elevate and stabilize the fluid temperature to meet building requirements [16,17]. Both the determined system parameters (including the building heat demand, the supply temperature on the user side, the temperature level of the geothermal source and the performance of the geothermal heat pump) and the design parameters (the working fluid, compressor efficiency, and heat exchanger pinch points) essentially determine the amount of thermal energy extracted from the subsurface. For example, in a deep closed-loop system, a large drop in outflow temperature can be observed within a short period of operation [18]. This will lead to a dynamic change in the performance of the geothermal heat pump. Therefore, the thermal interaction between the subsurface loop and the heat pump has to be taken into account during the design and optimization of DUBHE-coupled geothermal heat pump systems. The appropriate design and control optimization are crucial to decrease the payback period and boost the application of the system [19].

Various parameters can influence the performance of a ground-source heat pump (GSHP), including subsurface properties, climate conditions, the geometry of the ground heat exchanger, the parameters of the heat pump unit, and the supplementary heat or cold sources. Nevertheless, most of the research focused only on the subsurface closed-loop BHE part [20,21] or used an equivalent Coefficient of Performance (COP) to simplify the representation of the coupled heat pump [22–24]. In both approaches, the transient interaction of the heat pump off-design performance with the subsurface loop cannot be simulated and simultaneously quantified. Pan et al. [25] conducted a sensitivity analysis of the DBHE design parameters. These parameters included the outer pipe diameter, inner pipe diameter, flow rate, outer pipe materials, grout materials, and borehole depth. They optimized the DBHE design parameters under various geological conditions, focusing on the energy cost index but without taking the heat pump performance into account. Gascuel et al. [24] presented numerical simulations with

various designs of DBHEs and compared them for one year of continuous operation in a cold sedimentary basin. They found that the deepest and largest diameter wells perform best for the subsurface closed loop. However, the COP of a heat pump in their model typically varies depending on the outlet temperature of DBHEs linearly. Wang et al. [26] mentioned they optimized the operation of DBHE coupled with ground source heat pump systems but did not present the coupling scheme and detailed design parameters of the geothermal heat pump in numerical simulations. Brown et al. [27] used a simplified COP curve to quantify the heat pump performance when coupled to the DBHE loop, while such fitted COP curves have a limited range of validity.

Focusing on the heat pump system alone, Nikitin et al. [28] applied a Pareto-based multi-objective optimization method to enhance the system performance, considering energy, exergy, economic, and environmental factors. Schlosser et al. [29] and Jesper et al. [30] reviewed the selection of commercially available industrial heat pumps. They concluded that different working fluids have different operating ranges and performances, indicating that fluid selection is important for the DBHE-coupled geothermal heat pump and that some working fluids could lead to low efficiency when using fluctuating heat sources from subsurface loops. Chen et al. [31,32] developed a coupled model to quantify hydraulic and energy redistribution within a BHE array. This model involved simulating the pipe network in the ground using the software Thermal Engineering Systems in Python (TESPy) [33]. Notably, this model focused on the BHE array system and did not incorporate the real heat pump design. Using the same software, TESPy, Chen et al. [34] developed a general model to design and optimize the organic Rankine cycle power plant to use a two-phase geothermal heat source. However, the heat source condition is assumed to be constant and fixed in design and optimization. Pfeiffer et al. [35] and Gasanzade et al. [36] examined the interactions between a coupled power plant and a geo-storage system within porous media, focusing on compressed air energy storage. In addition, Dong et al. [37] developed an economic, energetic, and environmental evaluation algorithm for a hybrid mid-depth geothermal heating system. Their analysis was based on the key assumption of constant heat pump performance throughout the system's lifespan while not taking into account the influence of transient interactions between the heat pump and the subsurface loop. In terms of the economic and environmental implications of the DBHE-coupled geothermal system, Bae and Nam [38] conducted an analysis of the system's life-cycle climate performance. Their findings revealed that intermittent operation could decrease the total cost by as much as 18.7%, but it also led to an 11.8% increase in total carbon emissions.

In most numerical studies investigating the heating system with the heat source of closed-loop borehole heat exchangers, the boundary conditions for the subsurface are imposed as either the constant injection temperature or the constant heat extraction power [39–42]. When the flow rate of the closed loop in the subsurface pipes is fixed and the variation of thermal properties of the circulation fluid is neglected, the boundary condition of the constant heat extraction power is equivalent to the constant temperature difference between the inlet and outlet of the closed-loop system. These assumptions of the boundary condition in numerical models can evaluate tentative heat extraction capacity but are far from the real operation condition in a real heating system. These models that focus only on the subsurface loop will provide underestimation results of the heat extraction capacity and the sustainability of the subsurface loops. When the thermodynamic heat pump model is simultaneously simulated, the performance of the heat pump and the thermal performance response of the subsurface loop automatically harmonize to meet the system's heat demand. In terms of the amount of heat load on the subsurface loop, it will be redistributed between the heat pump and the subsurface closed loops in the operation. These features cannot be simulated and quantified by the independent subsurface model or the GSHP model with fixed heat source conditions. Behind these considerations lie three key scientific questions that can only be addressed using the integrated DUBHE-coupled heat pump system. What is the difference in thermal response performance estimated by the integrated model considering the interactions and thermal load redistribution behavior between the heat pump and the underground DUBHE? What is the effect of working fluid selection on the heat pump in a coupled DUBHE heating system from a thermal load redistribution perspective? What is the performance of the DUBHE-coupled heat pump system under the different control strategies, and how does the coupled system perform in typical operation patterns to support district heating systems?

To answer these scientific questions, a fully validated DUBHE model constructed in OpenGeoSys (OGS) [43,44] is coupled with a thermodynamic heat pump model in TESPy [33]. The interface between these two models is made using the pybind11 library [45] as described in Section 2. The validated model and the design of the heat pump are illustrated in Section 3. Subsequently, in Section 4, a comprehensive analysis is carried out on the interaction between subsurface DUBHE and the heat pump system. This analysis covers various aspects, including the impact of different heating loads on the performance of the DUBHE-coupled heat pump system, the influence of the working fluid, and the feed flow temperature in the geothermal heat pump. Then, two distinct control strategies are further analyzed in Section 4. Based on a typical heating demand time series, two operational settings of the system in the district heating system are simulated and compared in Section 5. The buffer effect of the redistribution of heat power is emphasized between the heat pump and the DUBHE system. Finally, the conclusions are drawn in Section 6.

2. Methodology

2.1. Subsurface DUBHE model

For DUBHE systems shown in the reference of Chen et al. [7] and Jiang et al. [12], three governing equations have to be included to quantify the physical process in the borehole and surrounding formations, which correspond to the energy balance in each compartment.

In surrounding subsurface geological formations, with intrinsic soil/rock specific heat capacity c_s, intrinsic soil/rock density ρ_s and soil/rock porosity ϵ, the evolution of soil/rock temperature T_s is determined by the following governing equation considering both heat advection and conduction,

$$\left[\epsilon\rho_w c_w + (1-\epsilon)\rho_s c_s\right]\frac{\partial T_s}{\partial t} + \rho_w c_w \mathbf{v}_w \cdot \nabla T_s - \nabla\cdot\left(\Lambda_s \cdot \nabla T_s\right) = H_s, \tag{1}$$

where c_w, ρ_w, and $\mathbf{v}_w$ refer to the specific heat capacity, density, and Darcy velocity of groundwater, respectively. Λ_s denotes the thermal hydrodynamic dispersion and H_s represents the heat source and sink terms. The following equation then gives the heat flux between soil/rock and the borehole,

$$q_s = -\Phi_{gs}\left(T_g - T_s\right) \text{ on } \Gamma_s, \tag{2}$$

where Γ_s is the boundary between soil/rock and borehole, Φ_{gs} is the thermal resistance between the soil/rock and the grout inside the borehole, and T_g is the grout temperature inside the borehole.

For the grout compartment surrounding the pipe inside the borehole, the heat transport process is assumed to be dominated only by heat conduction,

$$\rho_g c_g \frac{\partial T_g}{\partial t} - \nabla\cdot\left(\lambda_g \nabla T_g\right) = H_g \tag{3}$$

with Robin type of boundary condition (BC) :

$$q_g = -\Phi_{gs}\left(T_s - T_g\right) - \Phi_{fg}\left(T_f - T_g\right) \text{ on } \Gamma_g. \tag{4}$$

The heat exchange term Φ_{fg} is the thermal resistance between the circulation fluid T_f and the grout T_g. Detailed calculations of the heat exchange coefficients Φ_{fg} and Φ_{gs} can be found in Diersch et al. [46].

For the circulation fluid inside the pipe, the heat transport process is mainly dominated by the heat advection of the circulation fluid with a flow velocity of $\mathbf{v}_\mathrm{f}$,

$$\rho_\mathrm{f} c_\mathrm{f} \frac{\partial T_\mathrm{f}}{\partial t} + \rho_\mathrm{f} c_\mathrm{f} \mathbf{v}_\mathrm{f} \cdot \nabla T_\mathrm{f} - \nabla \cdot \left(\Lambda_\mathrm{f} \cdot \nabla T_\mathrm{f} \right) = H_\mathrm{f} \tag{5}$$

with Robin type of BC :

$$q_\mathrm{f} = -\Phi_\mathrm{fg} \left(T_\mathrm{g} - T_\mathrm{f} \right) \text{ on } \Gamma_\mathrm{f}, \tag{6}$$

in which the hydrodynamic thermal dispersion can be written as,

$$\Lambda_\mathrm{f} = \left(\lambda_\mathrm{f} + \rho_\mathrm{f} c_\mathrm{f} \beta_\mathrm{L} \| \mathbf{v}_\mathrm{f} \| \right) \tag{7}$$

where λ_f, ρ_f, c_f denote the heat conductivity, density, and specific heat capacity of the circulation fluid. Finally, β_L refers to the longitudinal heat dispersivity coefficient.

The DUBHE model was implemented in the OGS software using a dual-continuum approach [7,46]. The two heat transport equations inside the borehole are solved on 1D line elements, and the surrounding soil/rock heat transport equation is solved on 3D elements. The implemented model has already been successfully verified against analytical solutions and documented in [7,47] in detail.

2.2. Heat pump model

TESPy is a free and open-source software for simulating the steady-state operation of thermal engineering applications [33]. The library provides various fundamental components, such as pumps, heat exchangers, turbomachinery, and piping components. These components can be interconnected to construct a comprehensive heat pump model. Each component adheres to basic balance equations for mass, energy, and hydraulic pressure, and can be customized with specific balance equations and constraints according to user requirements. Moreover, TESPy offers access to a wide spectrum of different working fluids by implementing the CoolProp library [48] as its thermodynamic property engine.

For this study, the heat pump models are built with standard components from TESPy, which are `SimpleHeatExchanger` representing the condenser, `HeatExchanger` representing all other heat exchangers, as well as the `Compressor`, `Valve`, and `Pump` classes.

All components are assumed to be adiabatic to the environment. The `SimpleHeatExchanger` supplies the heat demand side of the heat pump with the respective heat, but only condensation is part of the modeling. The cold side of that heat exchanger is excluded from the model. For the `HeatExchanger` model, the amount of heat transferred from the hot fluid with subscript 1 is equal to the heat absorbed by the cold fluid with subscript 2 in Eq. (8). The actual amount of heat transferred $\dot{Q}$ is then calculated with Eq. (9).

$$0 = \dot{m}_{\mathrm{in},1} \cdot \left(h_{\mathrm{out},1} - h_{\mathrm{in},1} \right) - \dot{m}_{\mathrm{in},2} \cdot \left(h_{\mathrm{out},2} - h_{\mathrm{in},2} \right) \tag{8}$$

$$\dot{Q} = \dot{m}_{\mathrm{in},1} \cdot \left(h_{\mathrm{out},1} - h_{\mathrm{in},1} \right) \tag{9}$$

Furthermore, one of the important design parameters of a heat exchanger is the terminal temperature difference ΔT_t. As the design of all heat exchangers modeled in this study is in counter-current flow, $\Delta T_{\mathrm{t,u}}$ defines the upper temperature difference between the hot side fluid entering the heat exchanger and the cold side fluid leaving it, see Eq. (10). Analogously, $\Delta T_{\mathrm{t,l}}$ in Eq. (11) refers to the temperature difference between the hot side fluid that leaves the component and the cold side fluid that enters it. For the evaporator, $\Delta T_{\mathrm{t,l}}$ becomes ΔT_{pp}, which refers to the pinch point temperature difference.

$$0 = \Delta T_{\mathrm{t,u}} - T \left(p_{\mathrm{in},1}, h_{\mathrm{in},1} \right) + T_{\mathrm{out},2} \tag{10}$$

$$0 = \Delta T_{\mathrm{t,l}} - T \left(p_{\mathrm{out},1}, h_{\mathrm{out},1} \right) + T_{\mathrm{in},2} \tag{11}$$

To calculate the pressure loss in the heat exchangers, a detailed knowledge of the dimensions and structure of the devices is required. As this is not the main focus of this study, pressure losses in these components are thus neglected.

To model the part load operation of the heat exchangers, the kA value is calculated based on the design conditions. Then, the calculated value is applied to the model with a correction based on the mass flow on both sides of the heat exchanger. In the condenser, a constant temperature difference between the condensing working fluid and the heat demand side is assumed.

The compressor and pump are modeled using the isentropic efficiency $\eta_{\mathrm{s,cmp}}$ equation for processes of pressure increase, see Eq. (12). The resulting/necessary mechanical work rate $\dot{W}_{\mathrm{t,mech}}$ can be calculated from the steady-state energy balance, see Eq. (13). The electrical mechanical efficiency is assumed to be 1 for simplification. The expansion process of the working fluid in the valve is assumed to be adiabatic and isenthalpic.

$$\eta_{\mathrm{s,cmp}} = \frac{h_2 - h_1}{h \left[p_2, s \left(p_1, h_1 \right) \right] - h_1} \tag{12}$$

$$\dot{W}_{\mathrm{el}} = \dot{W}_{\mathrm{t,mech}} = \dot{m} \cdot \left(h_2 - h_1 \right) \tag{13}$$

For part load modeling of these components, the isentropic efficiency is modified with a lookup table based on the mass flow, similar to the approach for the heat exchangers.

In addition to the component-related equations, specifications of the fluid properties, for example, temperature, pressure, or vapor mass fraction, can be applied to the connections between the components. All assumptions of the applied models are available in Section 3. The governing equations of the complete model are then solved simultaneously with Newton's method in the TESPy software. For more details on the concrete implementation, please refer to the online documentation [49].

2.3. Model coupling

The transient data exchange between the DUBHE model in OGS and the thermodynamic heat pump model in TESPy is achieved by the pybind library [45]. The coupling calculation scheme is depicted in Fig. 1. The workflow is initialized by setting up the subsurface model initial boundary conditions and the heat pump model topology and design, i.e. the flow sheet of the plant and the component specifications such as the design isentropic efficiency of the compressor. In addition, a heat demand time series is used as input, which governs the heat pump operation.

For model coupling, the BHE outflow temperature $T_{\mathrm{BHE,out}}$ and the flow rate of the DUBHE loop $\dot{V}_{BHE,in}$, as well as the reinjection temperature to the subsurface DUBHE $T_{\mathrm{BHE,in}}$ are exchanged between the two models. The convergence criterion of the integrated simulation is the subsurface temperature (including the DUBHE outflow temperature), which is controlled by the Picard iteration in the OGS subsurface model.

For the control of the system, two different operation modes are available: In (a) the volumetric flow rate in DUBHE $\dot{V}_{\mathrm{BHE,in}}$ is set to a constant value. Consequently, the heat pump model is used to calculate the DUBHE inflow temperature $T_{\mathrm{BHE,in}}$ based on the volumetric flow rate and the provided heat production $\dot{Q}$. For the control strategy (b), the temperature change between the DUBHE outflow and the inflow ΔT_{BHE} is set constant. In this way, the heat pump calculates the required DUBHE volumetric flow and the DUBHE inflow temperature. Then both values are passed to the subsurface model, which determines the BHE outflow temperature. In both operation modes, the heat pump model is not executed when the heat demand is zero. For this, the subsurface model is only simulated heat recovery process in a shut-in mode.

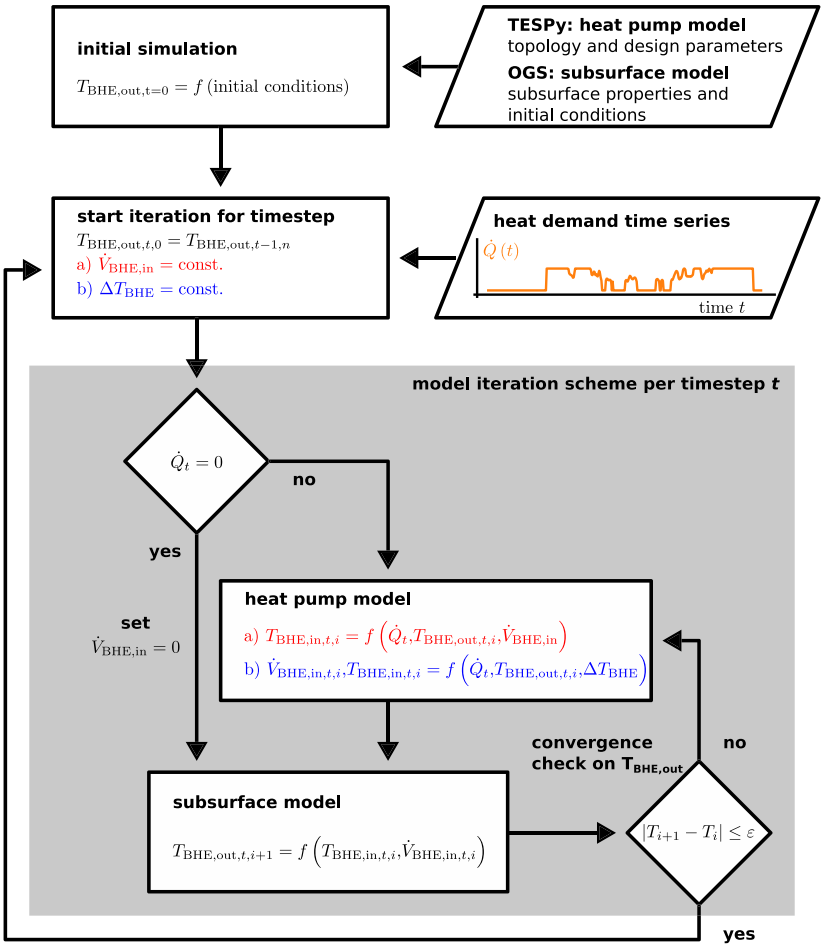

Fig. 1. The coupling scheme and computational workflow in the DUBHE coupled heat pump system.

3. System description

3.1. The subsurface DUBHE system

The pilot-scale heating project incorporating a DUBHE loop was constructed in Xi'an City, China, in 2018. The geometry and geothermal temperature of the subsurface loop are illustrated in Fig. 2. Following testing and commissioning, the DUBHE heating system officially commenced operation in the Winter of 2020. For further details on the project and the validation model setup according to the real geological structure and properties of the pilot project, see [50].

Throughout the monitored period, the average flow rate of the system remains at 44.3 m^3/h, except during short-term shutdowns. The monitored inflow temperature is depicted in Fig. 3 and serves as the boundary condition in the validation model. The simulated outflow temperature is then compared to the monitored data and presented in the same figure. The mean difference between the monitored outflow temperature and the simulated results is 1.1 °C (approximately 3.12%) during the first 10 days. However, after 30 days of operation, the simulated results closely match the monitoring data, with a temperature difference of only 0.1 °C (0.63%), which is well within the accuracy of the monitoring sensors. This demonstrates that the numerical model accurately captures the heat performance of the subsurface DUBHE loop. Thus, the validated DUBHE model can be utilized further as a heat source to investigate the dynamic coupling performance with the geothermal heat pump.

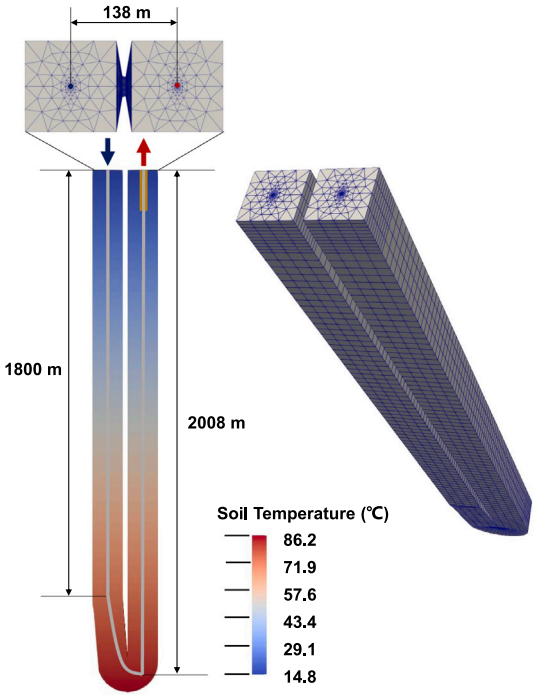

Fig. 2. Geometry and initial geothermal temperature distribution of the validation model.

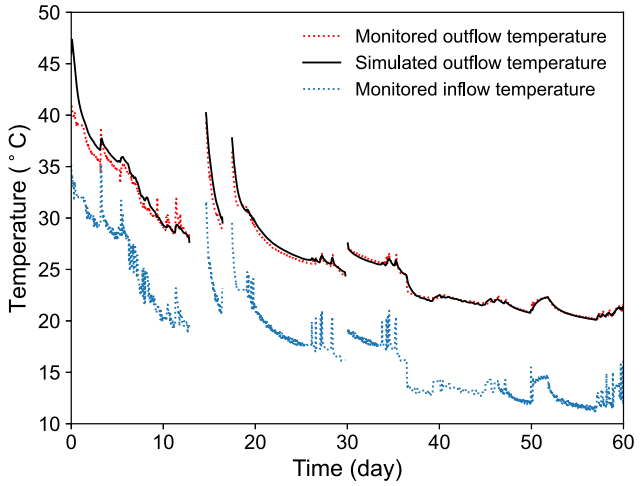

Fig. 3. Validated results of the DUBHE model for the subsurface.

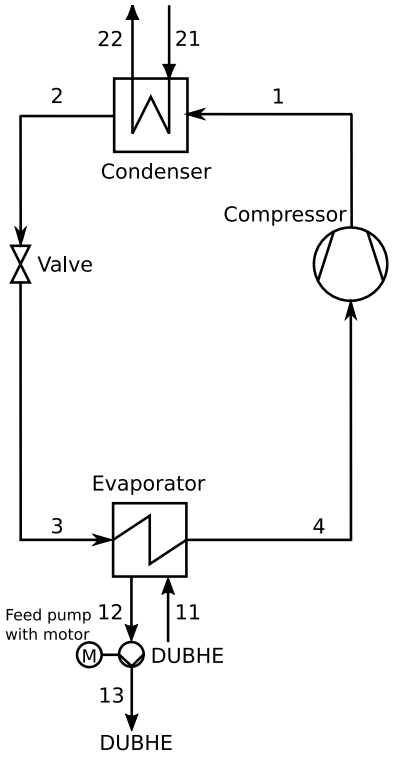

Fig. 4. The design of the heat pump topological structure.

3.2. The geothermal heat pump system

The topological structure of the geothermal heat pump illustrated in Fig. 4 is designed and will be coupled with the DUBHE system in this study. The detailed design parameters are listed in Table 1 to use the heat source temperature from the validated subsurface DUBHE model.

In the DUBHE-coupled heat pump model, the subsurface model contains 39,358 elements in total and it takes around 23 min to complete the simulations of 120 days (one heating season) with 168 time steps. The heat pump model as well as the model coupling overhead play a minor role in the computational effort. The model is simulated using a small workstation equipped with an i9-12900K processor and 32 GB of memory using to the OGS release version [44].[1] When simulating 1-year scenarios that are integrated into the heating system, more time steps are needed for the daily-averaged operation. For these cases, the computational time is about 52 minutes.

Table 1
Process design parameters for the heat pump.

Parameter	Symbol	Unit	Value
Isentropic efficiency of compressor	η_s	%	85
Isentropic efficiency of the circulation pump	$\eta_{s,cp}$	%	75
Lower terminal temperature difference of evaporator	$ttd_{l,e}$	°C	5
Electric-mechanical efficiency of pump motor	$\eta_{el,m}$	%	97
Required feed flow temperature	T_{22}	°C	65
Lower terminal temperature difference of condenser	$ttd_{l,c}$	°C	3

3.3. Simulation scenarios

Based on the fully validated subsurface DUBHE model, the thermodynamic heat pump model is coupled and simulated in a series of different scenarios, simulating different thermal response performance of the DUBHE to the heat pump operation. The various operation patterns of the DUBHE-coupled heat pump in a district heating system are compared from the performance response and energy point of view. In the previous study of model validation and extended scenarios [50], the subsurface DUBHE system was operated in different short- and long-term scenarios. The DUBHE was found to have a sustainable heat extraction rate of approximately 480 kW solely from the subsurface loop. Based on the evaluation, the DUBHE-coupled heat pump model is first simulated with five different thermal load values, i.e. 580 kW, 680 kW, 780 kW, 880 kW with a fixed DUBHE flow rate. The heat extraction performance of the subsurface DUBHE loop and the heat pump during one heating season (120 days) is presented in Section 4.1 to show the system heating capacity for buildings. The different working fluids in the heat pump could result in a different performance of the heat pump and its thermal load redistribution capacity. Therefore, under a sustainable heat extraction rate in the DUBHE-coupled heat pump system, the influence of the selection of the working fluid in the heat pump design is investigated subsequently in Section 4.2. The potential working fluid for the heat pump in this study includes R410A, R600, R1234ze(E), and R290. When the DUBHE-coupled heat pump system is integrated into a district heating system, the required feed flow temperature fluctuates along with the ambient temperature. Therefore, to illustrate the effect of the feed flow temperature in the operation of the system, the different feed flow temperatures are given as an additional constraint in Section 4.3. The control strategy of the coupled system and the thermal load distribution are determined by the heat pump, which is achieved by specifying the re-injection temperature or the flow rate to the subsurface DUBHE loop. The detailed influence of these two control strategies is investigated in Sections 4.4 and 4.5.

After analyzing the characteristics of these two control strategies, the integrated operation of the DUBHE-coupled heat pump in a typical district heating system is simulated in Section 5. In an integrated operation of one year, the required feed flow temperature and various thermal loads on the DUBHE-coupled heat pump system are specified according to the two main operation patterns in summer and winter. The performance and amount of energy provided by the heat pump and subsurface geothermal energy are analyzed and quantified in the district heating system.

A typical heat demand curve for district heating is taken into account. Triebs et al. [51] and Triebs and Tsatsaronis [52] collected data from more than 80 district heating systems in Germany and derived a normalized heat demand time series together with the respective ambient temperature. Next, this time series is scaled to a peak

[1] https://doi.org/10.5281/zenodo.11652195.

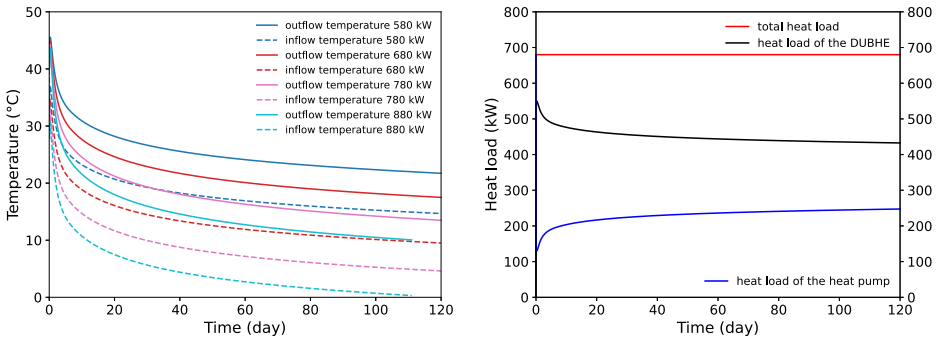

Fig. 5. (a) The inflow and outflow temperature evolution in one heating season (120 days) under different heat rates in the heat pump shown in Fig. 4 using the working fluid R410A. (b) The heat power redistribution phenomena of the DUBHE-coupled system with the total heat power of 680 kW.

load demand of 3 MW. The feed flow temperature of the system is calculated following the methodology of DIN 4747, 8.3.1 ("Gleitend-konstante Netzfahrweise"). In this study, the following assumptions for the temperature of the heat demand are made: 80 °C for the ambient temperature below −5 °C and 60 °C for the ambient temperature above 15 °C. For ambient temperatures in between, linear interpolation is applied.

To determine the operation patterns of the heat pump, a daily operation is assumed. Based on the daily mean duration of the heat demand curve for the summer operation pattern, the heat pump is considered the main source of heat. The heat pump is operated from March 21 to December 20 if the load is sufficiently high. For the winter operation pattern, the heat pump is considered the second heat provider (the base load is provided by a different technology). An offset of 800 kW is subtracted from the heat demand time series and the heat pump is operated based on the residual demand. The results of the two operation patterns are analyzed and discussed in Section 5.

4. Sensitivity analysis

4.1. Heating performance of the DUBHE-coupled heat pump system

In this section, four continuous heat loads, including 580 kW, 680 kW, 780 kW, 880 kW, are imposed on the DUBHE-coupled heat pump system for 120 days using the working fluid R410A. Under the four different thermal loads on the DUBHE-coupled heat pump system, the outflow and inflow temperatures of the DUBHE system are depicted in Fig. 5(a) for one heating season (120 days). It can be seen that the inflow temperature of the DUBHE loop in the coupled system is approaching 0 °C after around 110 days under the fixed thermal load of 880 kW. Once the freezing temperature is reached, the system cannot be operated anymore because pure water is used as the circulation fluid in the DUBHE loop. Therefore, the DUBHE-coupled geothermal system in this study cannot provide continuous heating demand when the fixed thermal load exceeds 880 kW over 120 days, even though the outflow temperature is still 9.9 °C. When we decrease the thermal load to 780 kW, the outflow temperature of the DUBHE increases by 3.6 °C, reaching 13.5 °C at the end of the season, along with the inflow temperature of 4.6 °C. Taking into account the decrease in the heat extraction performance in long-term operation with the heating and recovery season, the lowest inflow temperature is very possible to approach 0 °C. In this case, it is safer to conclude that the sustainable heating capacity of the DUBHE-coupled geothermal heat pump is below 780 kW. After 120 days, the outflow and inflow temperatures are 17.5 °C and 9.5 °C for the continuous heat production of 680 kW, respectively. When there is a lower heating demand from the heat pump at 580 kW, the inflow temperature is even 1.2 °C higher than the outflow temperature in the case with 780 kW heating demand. Therefore, the corresponding COP value of the heat pump is higher in this scenario.

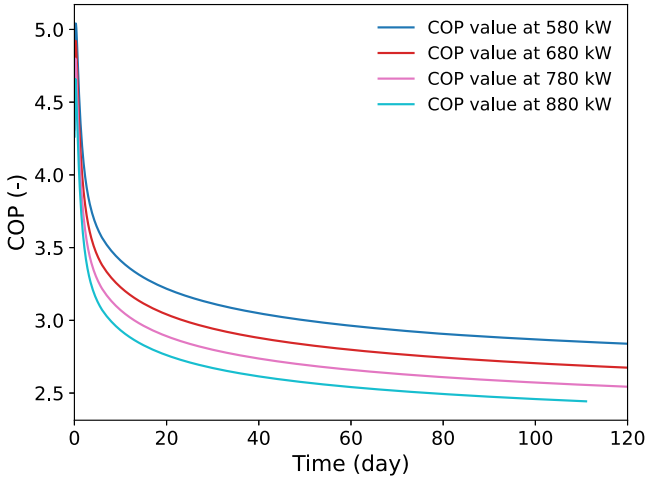

Fig. 6. The COP values of the heat pump in the off-design mode in one heating season (120 days) under different heating power in the heat pump over time.

Notably, when the total heat load of 680 kW is imposed in the DUBHE-coupled heat pump system, the actual heat power extracted from the DUBHE decreases from 549 kW to 433 kW in 120 days as shown in Fig. 5(b). The heat load on the DUBHE decreases by 116 kW in 120 days, which is approximately 21%. The thermal load redistribution between the DUBHE and the heat pump in the operation of the district heating system actually enhances the system's sustainability of operation, i.e., slowing down the decrease in the outflow temperature of the DUBHE system, as depicted in Fig. 5(b). As operational time accumulates, the outflow temperature of the DUBHE decreases and the heat power distributed on the heat pump increases, which decreases the actual heat load on the DUBHE system and vice versa. In this case, the DUBHE system will be operated more sustainably from the above zero-temperature perspective compared to the scenario with constant heat load on the DUBHE. The phenomenon of heat load redistribution during operations shows a buffer effect between the demand sectors and the subsurface system.

The specific change in the COP values of the heat pump during the operational time and against the outflow temperature of the DUBHE loop is illustrated in Fig. 6. The COP value is decreasing along with the heat source temperature decrement over 120 days. Specifically, the COP value decreases from 4.9 to 2.7 over 120 days under thermal load 680 kW. As expected, the change of the COP value with the heat source temperature/outflow temperature of the DUBHE loop maintains a nonlinear relationship.

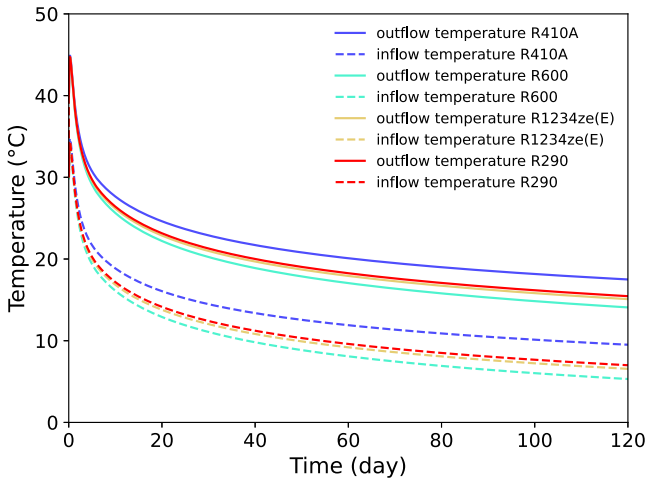

Fig. 7. The inflow and outflow temperature evolution in one heating season (120 days) with different working fluids in the heat pump shown in Fig. 4 under the heating power of 680 kW.

4.2. Effect of working fluid selection

In this section, four different working fluids are applied to the heat pump, including R410A, R600, R1234ze(E), and R290. When the thermal load on the geothermal heat pump is 680 kW, the evolution of the DUBHE inflow and outflow temperature is illustrated in Fig. 7 over the 120-day period. Observing the DUBHE outflow temperature, the R410A heat pump system has the highest values throughout the heating season. The outflow temperature difference of the coupled DUBHE between the R600 and R410A heat pumps reaches 3.4 °C after continuous operation of 120 days under the same thermal load of 680 kW in the coupled system. Therefore, less geothermal heat is extracted from the R410A heat pump system, which results in a worse performance of the heat pump and higher electricity consumption. The COP value of the R600 heat pump is 0.6 higher than that of the R410A.

The COP relationships with the DUBHE outflow temperature for the four selected working fluids are illustrated in Fig. 8(a). It shows that the R600 heat pump has the highest COP values among the four designs under the same DUBHE outflow temperature. The thermodynamic properties of the fluid lead to an inherently higher COP at the same temperature value. When there is a heat source temperature from the DUBHE loop with 35 °C, the COP value of the R600 heat pump is approximately 1.11 higher than that of R410A. More heat will be extracted through the DUBHE loop by the heat pump when the COP values are higher, or vice versa. Therefore, the R600 heat pump has the best performance from an economic perspective, while the R410A is the best considering the sustainability of the heat extraction of the system due to the lower heat load transferred to the DUBHE and the higher circulation temperature in the subsurface DUBHE loop. Similarly, in Fig. 8(b), it is observed that a COP value of 3.5 is reached after 42 days of operation using R600, and for R410A, this value can already be found after 4 days. Most importantly, although the COP advantage of R600 leads to a faster reduction in subsurface temperature as illustrated in Fig. 7, it is still retained at the high level during the entire operation time shown in Fig. 8(b).

4.3. Effect of feed flow temperature

Five different feed flow temperatures, i.e., 60 °C, 65 °C, 70 °C, 75 °C, 80 °C, are imposed on the DUBHE-coupled heat pump system in this section to show the performance change with the heating power of 680 kW. Throughout a heating season period, the evolution of the COP of the heat pump, the relationship between the COP values, and the outflow temperature of the DUBHE are shown in Fig. 9. Due to the high feed flow temperatures among the four scenarios, the working fluid of the heat pump is selected as R290.

As expected, COP values can increase as the feed flow temperature on the heat pump is lower. When the feed flow temperature increases from 60 to 80 °C, the COP value decreases by 0.70 after 120 days, but the outflow temperature increases by 5.06 °C. This is because a higher feed flow temperature requires a higher condensing temperature and, therefore, a pressure ratio between the evaporation and condensation sides of the working fluid in the heat pump, leading to a higher electricity consumption in the compressor. However, the low COP values decrease the amount of heat extracted from the subsurface; the outflow temperature of the DUBHE increases as a result of the heat load redistribution by the heat pump, confirming the observations made in the previous section.

4.4. Re-injection temperature control to the subsurface loop

Different flow rates of the DUBHE loop are specified manually in this section. The inflow/re-injection temperature of the DUBHE loop is controlled by the heat pump based on the heating demand, the DUBHE production temperature, and the specified flow rate of the DUBHE loop. Under this control strategy, the resulting temperature change from the operation is shown in Fig. 10.

Generally, lowering the flow rate in the DUBHE results in an increase in the outflow temperature because there is more time for the circulation fluid to extract geothermal energy. This effect alone would lead to a higher COP in the heat pump. However, to meet the heat demand independently of the flow rate in the DUBHE, a lower flow rate in the DUBHE loop will also lead to a higher temperature difference between the DUBHE inflow and outflow. Therefore, the evaporation temperature decreases and the COP of the system decreases as well, similar to the effect of increasing the heat demand temperature. The pressure ratio between condensation and evaporation in the heat pump is increased with a decrease in the re-injection temperature. For the system to benefit, i.e. operate at higher COP, from the higher outflow temperature of the DUBHE in low-flow-rate operation, the heat demand has to be lowered simultaneously. To be specific, the outflow temperature of the DUBHE loop is 15.3 °C, 17.5 °C and 21.6 °C after 120 days, when the flow rate of the DUBHE loop is 0.0259 m^3/s, 0.012 95 m^3/s, and 0.006 475 m^3/s, respectively. The inflow temperature of the DUBHE loop is 11.2 °C, 9.5 °C, and 6.1 °C, accounting for the temperature difference of 4.1 °C, 8.0 °C, and 15.5 °C.

4.5. Flow rate control to the subsurface loop

In this section, the control strategy is changed to have a fixed temperature difference between the inflow and outflow of the DUBHE loop, which is the temperature difference on the hot side of the evaporator in the heat pump. The flow rates of the DUBHE loop are then adjusted automatically according to the heat pump performance. The DUBHE flow rate responds to the operation of the heat pump under the specific heating power. In one heating season, the outflow temperature is depicted in Fig. 11(a) as well as the required flow rate of the DUBHE loop (see Fig. 11(b)).

It can be found that both the outflow temperature and the required flow rate of the DUBHE loop are dynamically changed when the temperature difference is low. Under a temperature difference of 5 °C for the DUBHE loop, the flow rate decreases from 0.0271 m^3/s to 0.0209 m^3/s, the outflow temperature is 15.8 °C (decreased by 28.3 °C) after 120 days. When the temperature difference is fixed at 10 °C, the outflow temperature becomes 18.6 °C (decreased by 26.3 °C) after 120 days, and the flow rate decreases from 0.0132 m^3/s to 0.0103 m^3/s. When there is a lower temperature difference, the outflow temperature is lower throughout the heating season, while the inflow temperature is higher.

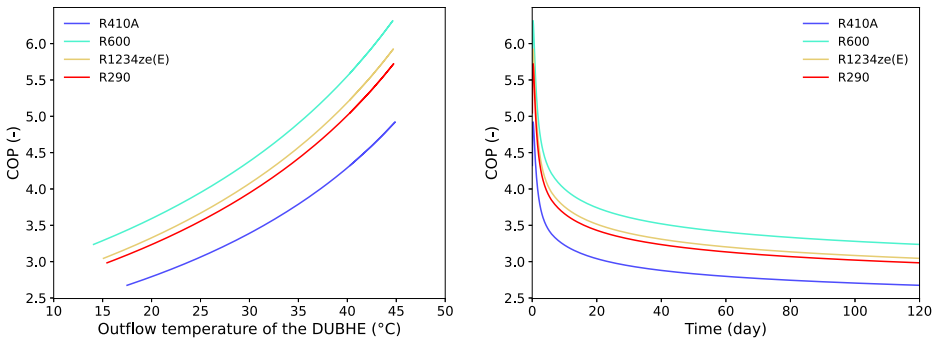

Fig. 8. The COP values of the heat pump in the off-design mode in one heating season (120 days) with different working fluids in the heat pump: (a) Over time and (b) outflow temperature of the DUBHE.

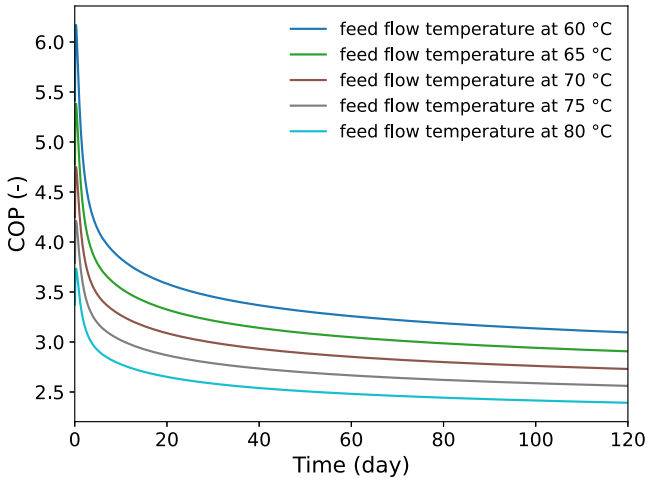

Fig. 9. The working fluids of R290 in the heat pump under the total heating power of 680 kW in one heating season (120 days): The COP changes over the operational time.

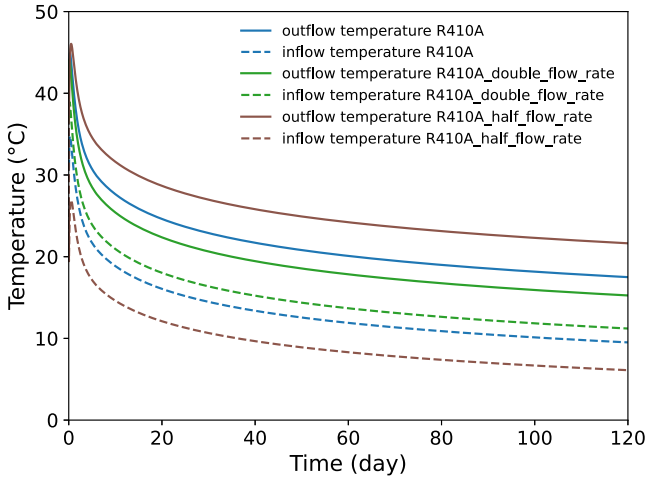

Fig. 10. The working fluid R410A in a heat pump under the total heating power of 680 kW during one heating season (120 days): The DUBHE inflow and outflow temperature evolution for three different flow rates.

5. Integrated operation in a district heating system

In this section, the DUBHE-coupled heat pump is integrated into a heating supply system. The heat pump operation patterns are derived from a typical heating demand time series for the typical district heating system in Germany [51,52]. The type of district heating system considered in this case study usually includes a basic demand for domestic hot water. Therefore, there is a summer load, albeit much lower than the winter load (as seen from the load curves in Fig. 12).

5.1. System setup

To ensure a minimum up-time or down-time of one day for the DUBHE system, the hourly demand data are first aggregated to the daily mean values. The first operation pattern is from spring to fall (summer case), from 79th to 354th day of the year. The heating demand from a district heating system and the actual heating load on the DUBHE-coupled heat pump system are depicted in Fig. 12(a). The heat pump provides 700 kW when the district heat demand is greater than 700 kW. The DUBHE-coupled heat pump system will supply all the heat demand if it is less than 700 kW and greater than its minimum allowable load of 280 kW. If the heat demand from the district heating system is less than 280 kW, the thermal load on the DUBHE-coupled system becomes 0 kW, keeping it in shut-down state. The total amount of heat production following the summer schedule will be 3053 MWh. The second operation pattern runs mainly in winter, as shown in Fig. 12(b). For the winter case, an offset of 800 kW is applied to the heat demand curve to account for a base load, which is not supplied by the heat pump. The residual heat demand is then calculated and supplied by the heat pump following the same rules as in the summer operation pattern. The total amount of heat to be provided by the heat pump is 2473 MWh, which is 19% lower than in the summer operation schedule.

In both cases, the feed flow temperature is assumed to be ambient dependent and decreases linearly from 80 °C to 60 °C with an increase in the ambient temperature from −5 °C to 15 °C. Due to the high feed flow temperature, R410A is infeasible as a working fluid. Instead, R290 is selected to present a moderate case (see Fig. 7).

For numerical stability in the subsurface model, the coupled simulation uses a time step size of one hour on the first day, and of 4 h on the days two to five. Only after day six, the model continues to run with a time step size of 1 day, making the total number of time steps 413. It takes around 52 min to complete the simulations using a small workstation equipped with an i9-12900K processor and 32 GB of memory.

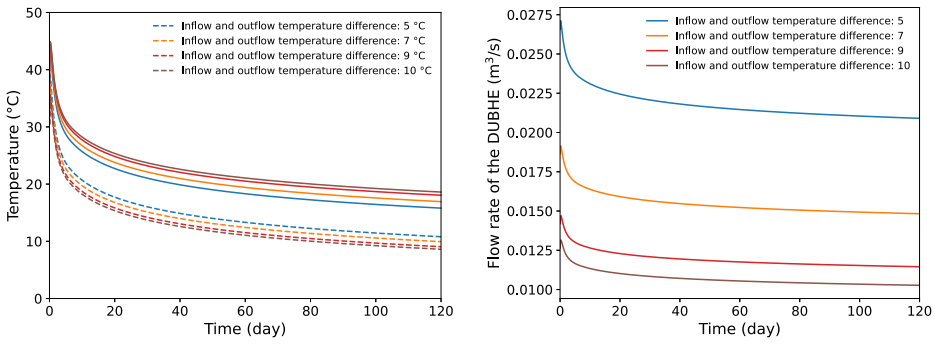

Fig. 11. The performance of the DUBHE system in one heating season (120 days) under the total heating power of 680 kW: (a) The evolution of DUBHE inflow and outflow temperature and (b) the required DUBHE flow rate by the heat pump.

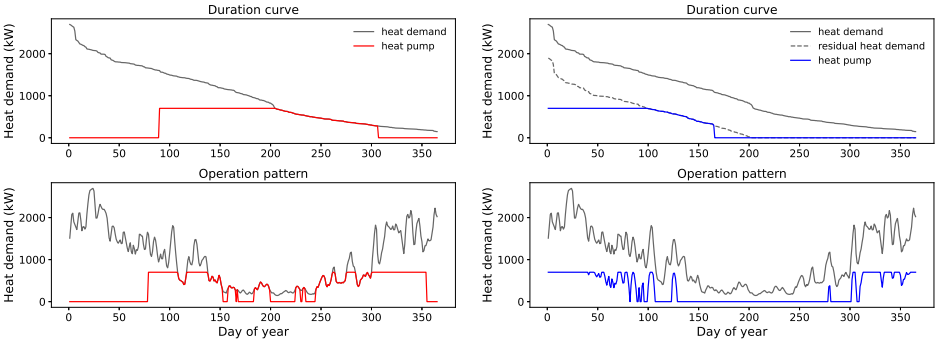

Fig. 12. The integrated operation of the DUBHE-coupled heat pump system in district heating: (a) During summer (over the period from the 79th to the 354th day of the year). (b) During winter, as the secondary plant providing the residual heat to the system after considering a base load 800 kW.

5.2. Performance

In this section, we will first provide an overview of the overall performance of the system and then investigate the influence factors on the annual COP of the heat pump in the different operation patterns. The annual shares of heat provided by the DUBHE and the work required by the heat pump in both operation strategies are shown in Fig. 13. As reported in Section 5.1, the total heat delivered to the heating demand is 3053 MWh in summer and 2473 MWh in winter. In the summer case 917 MWh of electrical work is required to power the system using a total of 2136 MWh heat from the subsurface. Overall, an annual COP of 3.33 is achieved. In the winter case, the total amount of heat provided to the system is lower, consequently also the total amount of electrical work (791 MWh) and the heat extracted from the subsurface (1683 MWh) are lower. The annual COP is 3.13.

In Fig. 14 the COP of the heat pump is shown temporally resolved to the time step size of one day (a) and as a boxplot (b). In the summer case, high COP values are achieved over extended periods of time, especially during the time when the heat demand is relatively low, or after the operation is restarted following a shut-down phase, confirming the investigation in Section 4.1. In the winter operation pattern, high COP values are observed especially when the heat pump is restarted after the summer shut-down period, or at the very beginning of the simulation period. Here, the COP then declines rapidly during the first days of operation. Overall, the winter case shows a lower spread in COP values ranging from 2.56 to 5.22. The summer pattern has a higher spread with a minimum value of 2.51 and a maximum value of 6.02. In addition, the median value of 3.48 (standard deviation 0.77) is significantly higher than in winter with 3.14 (standard deviation 0.44). In general, the COP is spread more widely in the summer operation

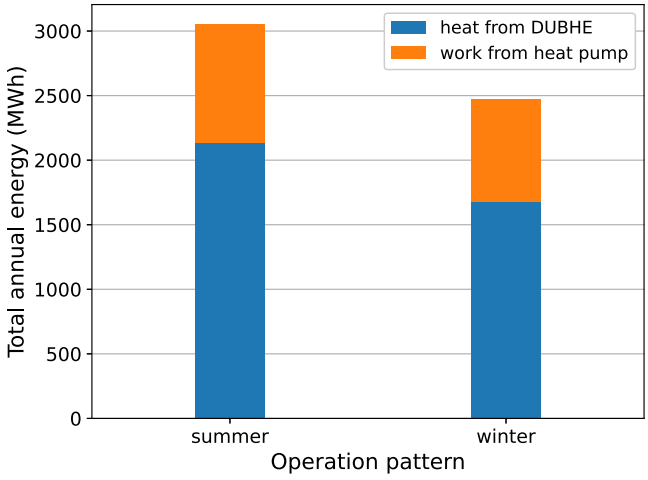

Fig. 13. The amount of total electricity demand of the heat pump and heat extracted from the subsurface in the two scenarios.

case (standard deviation of 0.73) compared to the winder operation case (standard deviation of 0.44).

In summary, while more heat is provided to the heating system in the summer case, the COP is higher simultaneously. This contrasts to the findings in Fig. 5, where a lower heat production rate (and therefore less heat extracted in total) shows a higher COP value.

Fig. 15 shows the daily inflow and outflow temperature of the DUBHE system for the whole year. The results of the summer case are shown in (a): From the first day to the 79th day of the year, the

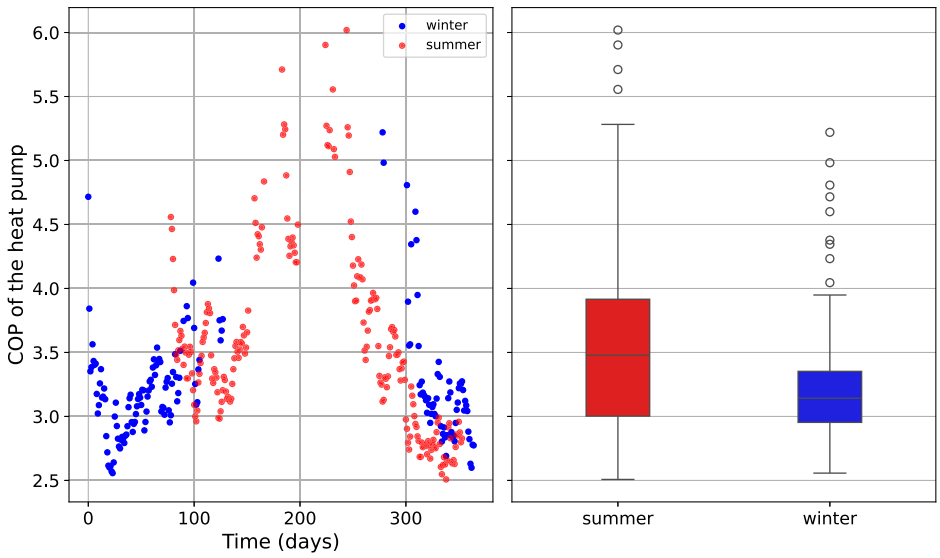

Fig. 14. COP values: (a) The heat pump COP distribution over the one year for the two different operation modes. (b) The statistic distribution of the COP values in the two cases.

DUBHE-coupled system is shut down. Therefore, the inflow and outflow temperatures of the DUBHE are the same as the initial formation temperature, kept at 15 °C. From the 79th day, water in the DUBHE loop of the subsurface starts to circulate, the outflow temperature suddenly increased due to the high-temperature circulation water in the bottom part of the loop. As the operation continues, the inflow and outflow temperatures respond to various heat loads required by the district heating system. When there is a lower heat load on the system, such as from 107th day to 114th day, the imposed heat load decreases from 683.2 to 414.6 kW, the outflow temperature of the DUBHE loop increases from 20.7 °C to 27.2 °C as a response. When no heat load is imposed on the system, circulation water is stopped in the DUBHE loop, but the heat transport (recovery) process continues. Therefore, during shutdown, the outflow and inflow temperatures remain the same and decrease because heat is transported from the circulation water to the low-temperature subsurface around the head of the DUBHE. After the operation pattern of the summer case in a whole year, the lowest outflow temperature of the DUBHE is 14.4 °C on the 353th day and the corresponding inflow temperature is 6.0 °C. In particular, the temperature level in the DUBHE remains relatively stable even during a continuous operation period from day 300 to day 353 as the outflow temperature drops from 17.9 to 14.4 °C.

For the winter case, the inflow and outflow temperature of the DUBHE system throughout the year is shown in Fig. 15(b). The system starts with relatively high outflow temperatures in the first days, which decrease rapidly and simultaneously with the COP during the first period of continuous operation in the first 50 days (also see Fig. 14). After that, the heat pump is operated at lower part-load shares and more intermittently and the temperature rises slightly. The heat pump is shut down from day 128 until day 300 with the exception of two days of operation on the days 278 and 279. In restart, the regeneration of the subsurface is visible by the elevated DUBHE outflow temperature level, which is more than 40 °C initially. After operation for one year, the outflow and inflow temperatures are 18.6 °C and 10.3 °C respectively, with a temperature difference of 8.3 °C. Due to the long recovery period in summer, the minimal BHE outflow temperature of 15.7 °C is slightly higher than in the summer case with 14.4 °C.

Although the subsurface temperature in the winter case is higher, the COP is lower compared to the summer operation. The reason for that is that the heat pump's performance strongly depends on the feed flow temperature of the heat demand as well and, with a minor effect, also on the part-load ratio of the heat pump itself. Since the dependence towards the BHE outflow temperature and heating demand feed flow temperature is the most significant, we will further investigate the effect of these factors on the COP. For that, Fig. 16 shows the histograms of the BHE outflow temperature (a) and the heat demand feed flow temperature (b). The BHE outflow temperature is slightly lower in the summer case due to the larger amount of total heat extracted from the subsurface. However, the difference from the winter case is very small: In the summer case, a mean value of 23.4 °C and a median value of 22.0 °C are observed, while the mean value is 24.8 °C and the median is 23.3 °C in the winter case. In contrast, the heat demand feed flow temperature has a stronger discrepancy between summer and winter in the frequency distribution. The summer case strongly leans towards the lower temperature limit of 60 °C (mean value 64.8 °C and median 63.6 °C) while the winter case is much more centered on the window ranging from 65 °C to 75 °C with a mean value of 70.2 °C and a median value of 69.9 °C. The much higher difference in the feed flow temperature distribution explains the high annual COP in summer compared to the winter case. In fact, the low amount of heat extraction from the subsurface in the winter case buffers the COP degradation. The difference between summer and winter operations will be more significant if the DUBHE temperature level is lower on top of the higher feed flow temperature regimes.

This trend can be confirmed by Fig. 17, which shows the dependency of COP on both the BHE outflow temperature (x-axis) and the heat demand temperature (y-axis) at the same time; a darker color indicates a lower COP. High COP values are achieved with simultaneously low heat demand and high BHE outflow temperature values, which occur more frequently in the summer case. It is noted that the lowest BHE outflow temperature values are also observed in the summer operation pattern, i.e. during the last hours of operation in the year. At the same time, the heating temperature starts to rise again and a strong degradation in COP is visible. It indicates that continuing the operation of the heat pump beyond that point in time could risk unsustainable operation of the system. Totally, the slightly higher DUBHE outflow temperature in the winter operation pattern buffers the COP depletion due to the high feed flow temperature values from the heat demand side.

5.3. Discussion

In this section, limitations in the modeling approach as well as potential improvements are discussed. First, in the coupled model in

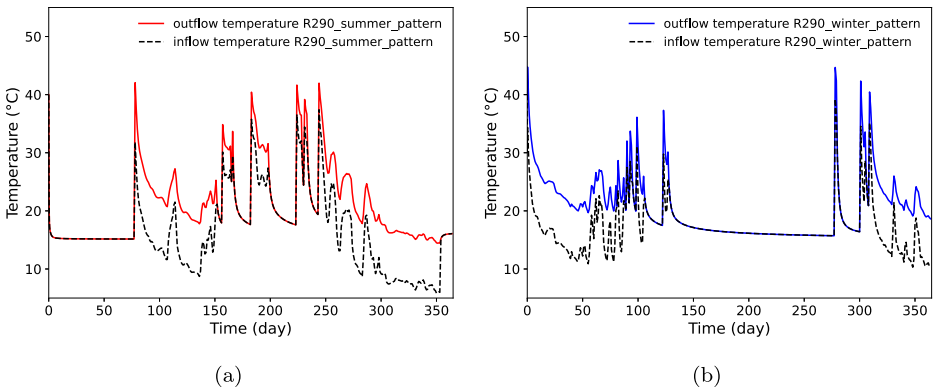

(a) (b)

Fig. 15. The inflow and outflow temperature of the DUBHE-coupled heat pump under the operation mode: (a) The summer case, and (b) the winter case.

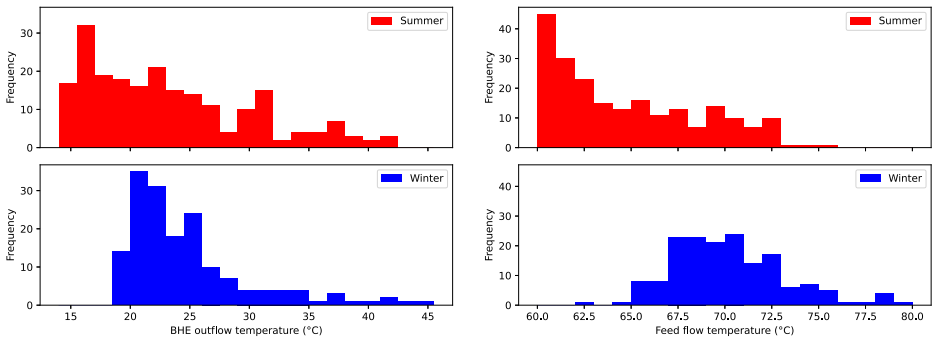

(a) (b)

Fig. 16. The comparison of the two operation patterns: (a) The outflow temperature frequency distribution of the DUBHE loop. (b) The feed flow temperature frequency distribution of the district heating system.

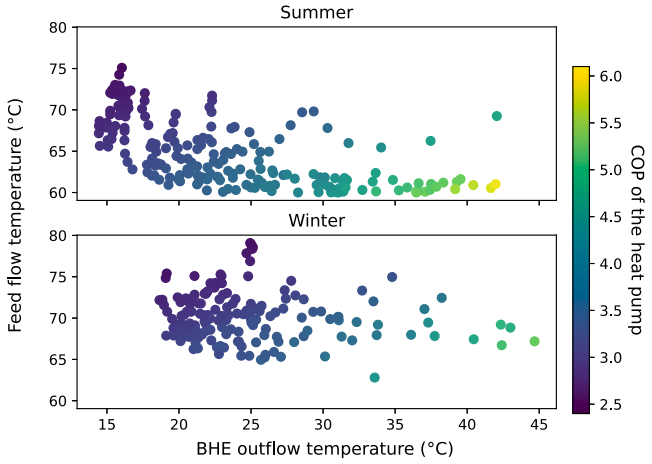

Fig. 17. The COP dependency of the outflow temperature of the DUBHE and the feed flow temperature in the two operation patterns.

this study, only the inflow and outflow temperatures and volumetric flow rate are transiently exchanged between the subsurface DBHE and the heat pump (see Fig. 1). In the subsurface DUBHE model, only heat transport processes are simulated in the closed loop and surrounding formations, and all thermal properties are assumed to be constant with a rational evaluation [22,42] as shown in the validation in Section 3. In the thermodynamic heat pump model, the loop is modeled based on the HEOS formulation for water properties [53], combined with the pressure values in the network. Therefore, the dynamic water properties calculated by the HEOS on the heat source side deviate slightly from the constant values set in the subsurface model. In addition to using the heat pump performance with annual COP values, the amount of energy extracted from the subsurface can also be directly calculated from the subsurface FEM-based DUBHE model. However, it is the mesh-dependent value because the temperature values have to be interpolated from the nodes to the elements [54]. In these circumstances, the extracted geothermal energy from the subsurface is accounted for 2173 MWh in the summer operation pattern, while it is 1703 MWh in the winter case, compared to 2136 MWh and 1683 MWh when calculated in the heat pump model. Based on the calculation of the subsurface model, the relative energy differences are 1.7% for the summer pattern and 1.1% for the winter pattern, respectively. These differences can be resolved in the future by implementing alternative back-ends in TESPy allowing the user to utilize constant density and heat capacity properties for subsurface circulating water or by including the mass and momentum balance equations in the subsurface model.

The second aspect is that the simulation is based on daily operation patterns. In reality, the actual heat demand patterns fluctuate significantly throughout the day, i.e., with peaks in the morning and in the early hours of the evening. Even more in the transition time between summer and winter, when the ambient temperature spreads widely during the day [55]. This requires the implementation of buffer storage as an interface between the heat pump and the heat demand. Heat losses in daily storage operation have not been considered and could play a key role in improving system sustainability and flexibility. In addition, the combination of heating in winter and cooling in summer could be beneficial for the BHE system [56]. However, heat storage can improve the heat extraction capacity only when the inlet temperature of the heat storage fluid is greater than the critical heat storage temperature. The average subsurface temperature around the 2008 m DUBHE is still very

high (around 50 °C) in the shutdown phase, making it very expensive to really inject heat into the subsurface by the DUBHE system in this study. Utilizing the BHE system for seasonal heat storage is more attractive in shallow or medium-depth applications [32,57,58]. In cases with large amounts of excess waste heat or abandoned solar/wind electricity, storing heat in deep geothermal applications could be economically feasible.

At last, the simulations in this study are limited to the first-year operation only. The lifetime of a geothermal heat pump project is expected to exceed 20 years, therefore long-term operation performance is important to evaluate system operational sustainability and economic feasibility [12,32]. The accumulated cold in the subsurface from previous years and the resulting performance decline significantly impact the system's heat redistribution capacity. Specifically, the temperature at the beginning of the second year operation will become lower than that in the first year in Fig. 15(b). In this study, the winter operation starts with the initial state of the system and results in a DUBHE outflow temperature within the range of 30 to 40 °C. At the end of the one-year operation, the DUBHE outflow temperature reaches only about 19 °C. Starting from that point, in the second year more than 80 days of continuous operation are aligned, which will result in much lower COP values than in the first year. For the summer case, this issue is less critical, because there are 80 days of shut-down until the operation starts again. This also indicates that the operation of a more frequent shutdown for the DUBHE is beneficial to the sustainability of the system.

6. Conclusions and outlook

In this work, a DUBHE-coupled heat pump model is implemented and developed based on the validated DUBHE model in the OGS software and the component-based simulation framework for thermal conversion processes TESPy. When considering the transient thermal response mechanism between the surface heat pump and the subsurface DUBHE loop, the heat redistribution behavior has been investigated in detail under different operation conditions and control strategies. Furthermore, two typical operation schedules have been analyzed to simulate the integration of the system into a typical district heating system. The main findings are summarized below.

- A well-fitting design of the components in a coupled BHE heat pump system can be achieved by an integrated assessment of the heat pump and the subsurface installation. The coupled model gives valuable insights on the interdependence of the operation, i.e., how the design choices in the heat pump and the projected operation pattern of the heat pump influence the sustainable operation of the BHE.
- The heat pump system distributes the total heat load in the DUBHE-coupled system according to its performance and the subsurface response. The maximum sustainable heating power of the system presented in this study is 780 kW in 120-day operation with the working fluid R410A and the required feed flow temperature of 65 °C in the heat pump. As the operation time increases, the COP of the heat pump decreases due to the decrease in the outflow temperature of the DUBHE, leading to a decrease in the heat load distributed to the subsurface DUBHE by the heat pump.
- The selection of the working fluid and the feed flow temperature of the heat pump have a significant impact on the performance of the entire system. For the R600 working fluid, although the advantage of COP leads to a fast reduction in the subsurface, it can be retained throughout the operation time. However, this over-extracted performance of the DUBHE poses a challenge to its sustainable operation regarding the circulation fluid temperature of the DUBHE.
- The system can be efficiently operated when the heat pump automatically controls the re-injection temperature of the DUBHE loop. When the flow rate of the DUBHE system doubles, the temperature difference between the inflow and outflow decreases by a factor of 1.95. However, this change is not linear, and further increases in the flow rate do not result in equivalent reductions in the temperature difference due to the variation of the heat pump performance.
- In the two operation patterns of the integrated system in the district heating system, the subsurface can provide around 70% of the total heat power to the district heating system. The average annual COP is 0.2 higher with frequent shutdown and low feed flow temperatures. In addition, the phenomenon of heat power redistribution during operations shows a buffer effect between the demand sectors and the subsurface system. The whole system illustrates significant flexibility in integrating into the district heating system.

To achieve a balanced system design and a highly efficient heating system, sufficient attention should be paid to the interdependence of the coupled system and the projected operational patterns. A performance evaluation of different heat pump designs, BHE designs and operational patterns can therefore help identify optimal system design. However, simulation of various scenarios requires a high computational effort.

CRediT authorship contribution statement

Chaofan Chen: Writing – original draft, Visualization, Software, Methodology, Investigation, Formal analysis, Conceptualization. **Francesco Witte:** Writing – review & editing, Visualization, Software, Methodology, Investigation, Formal analysis. **Reza Taherdangkoo:** Writing – review & editing, Investigation, Formal analysis. **Wanlong Cai:** Validation, Methodology, Investigation, Formal analysis. **Shuang Chen:** Software, Investigation. **Yanlong Kong:** Writing – review & editing, Investigation. **Haibing Shao:** Writing – review & editing, Investigation. **Mathias Hofmann:** Writing – review & editing, Methodology, Investigation. **Thomas Nagel:** Writing – review & editing, Resources, Project administration, Funding acquisition.

Declaration of competing interest

The authors declare that they have no known competing financial interests or personal relationships that could have appeared to influence the work reported in this paper.

Acknowledgments

This research is financially supported by the MineATES project (Nutzung grundwassererfüllter bergbaulicher Hohlräume als thermische Energiespeicher) funded by the German Federal Ministry of Education and Research (Grant No. 03G0910A), as well as the National Natural Science Foundation of China (No. 52306274), the China Postdoctoral Science Foundation, China (No. 2023TQ0262), and the Shaanxi Provincial Postdoctoral Research (No. 2023BSHYDZZ27).

Data availability

Data will be made available on request.

References

[1] Michopoulos A, Zachariadis T, Kyriakis N. Operation characteristics and experience of a ground source heat pump system with a vertical ground heat exchanger. Energy 2013;51:349–57.

[2] Alimonti C, Soldo E, Bocchetti D, Berardi D. The wellbore heat exchangers: A technical review. Renew Energy 2018;123:353–81.

[3] Cai W, Wang F, Jiang J, Wang Z, Liu J, Chen C. Long-term performance evaluation and economic analysis for deep borehole heat exchanger heating system in Weihe Basin. Front Earth Sci 2022;10:40.

[4] Li J, Bao L, Niu G, Miao Z, Guo X, Wang W. Research on renewable energy coupling system based on medium-deep ground temperature attenuation. Appl Energy 2024;353:122187.

[5] Gultekin A, Aydin M, Sisman A. Effects of arrangement geometry and number of boreholes on thermal interaction coefficient of multi-borehole heat exchangers. Appl Energy 2019;237:163–70.

[6] Cai W, Wang F, Chen S, Chen C, Liu J, Deng J, Kolditz O, Shao H. Analysis of heat extraction performance and long-term sustainability for multiple deep borehole heat exchanger array: A project-based study. Appl Energy 2021;289:116590.

[7] Chen C, Cai W, Naumov D, Tu K, Zhou H, Zhang Y, Kolditz O, Shao H. Numerical investigation on the capacity and efficiency of a deep enhanced U-tube borehole heat exchanger system for building heating. Renew Energy 2021;169:557–72.

[8] Malek AE, Adams BM, Rossi E, Schiegg HO, Saar MO. Techno-economic analysis of advanced geothermal systems (AGS). Renew Energy 2022;186:927–43.

[9] Kelly JJ, McDermott CI. Numerical modelling of a deep closed-loop geothermal system: evaluating the Eavor-Loop. AIMS Geosci 2022;8(2):175–213.

[10] Chen J, Feng S. Evaluating a large geothermal absorber's energy extraction and storage performance in a common geological condition. Appl Energy 2020;279:115793.

[11] Chong Q, Wang J, Gates ID. Evaluation of closed-loop U-Tube deep borehole heat exchanger in the Basal Cambrian Sandstone formation, Alberta, Canada. Geotherm Energy 2022;10(1):1–20.

[12] Jiang J, Wang F, Yang X, Zhang Y, Deng J, Wei Q, Cai W, Chen C. Evaluation of the long-term performance of the deep U-type borehole heat exchanger on different geological parameters using the Taguchi method. J Build Eng 2022;59:105122.

[13] Xiao D, Chen W, Li L, Gao R, Yang R, Tang H, Li G. Techno-economic coupling model of U-shaped closed-loop geothermal system. Geothermics 2022;105:102540.

[14] Blázquez CS, Martín AF, Nieto IM, García PC, Pérez LSS, González-Aguilera D. Analysis and study of different grouting materials in vertical geothermal closed-loop systems. Renew Energy 2017;114:1189–200.

[15] Sun F, Yao Y, Li G, Li X. Geothermal energy development by circulating CO2 in a U-shaped closed loop geothermal system. Energy Convers Manage 2018;174:971–82.

[16] Wang Z, Wang F, Liu J, Li Y, Wang M, Luo Y, Ma L, Zhu C, Cai W. Energy analysis and performance assessment of a hybrid deep borehole heat exchanger heating system with direct heating and coupled heat pump approaches. Energy Convers Manage 2023;276:116484.

[17] Qiu G, Li K, Cai W, Yu S. Optimization of an integrated system including a photovoltaic/thermal system and a ground source heat pump system for building energy supply in cold areas. Appl Energy 2023;349:121698.

[18] Wang X, Zhou C, Ni L. Experimental investigation on heat extraction performance of deep borehole heat exchanger for ground source heat pump systems in severe cold region. Geothermics 2022;105:102539.

[19] Ma Z, Xia L, Gong X, Kokogiannakis G, Wang S, Zhou X. Recent advances and development in optimal design and control of ground source heat pump systems. Renew Sustain Energy Rev 2020;131:110001.

[20] He Y, Bu X. A novel enhanced deep borehole heat exchanger for building heating. Appl Therm Eng 2020;178:115643.

[21] Li C, Guan Y, Liu J, Jiang C, Yang R, Hou X. Heat transfer performance of a deep ground heat exchanger for building heating in long-term service. Renew Energy 2020;166:20–34.

[22] Chen C, Shao H, Naumov D, Kong Y, Tu K, Kolditz O. Numerical investigation on the performance, sustainability, and efficiency of the deep borehole heat exchanger system for building heating. Geotherm Energy 2019;7(1):18.

[23] Zheng T, Shao H, Schelenz S, Hein P, Vienken T, Pang Z, Kolditz O, Nagel T. Efficiency and economic analysis of utilizing latent heat from groundwater freezing in the context of borehole heat exchanger coupled ground source heat pump systems. Appl Therm Eng 2016;105:314–26.

[24] Gascuel V, Raymond J, Rivard C, Marcil J-S, Comeau F-A. Design and optimization of deep coaxial borehole heat exchangers for cold sedimentary basins. Geothermics 2022;105:102504.

[25] Pan S, Kong Y, Chen C, Pang Z, Wang J. Optimization of the utilization of deep borehole heat exchangers. Geotherm Energy 2020;8:1–20.

[26] Wang Y, Wang Y, You S, Zheng X, Wei S. Operation optimization of the coaxial deep borehole heat exchanger coupled with ground source heat pump for building heating. Appl Therm Eng 2022;213:118656.

[27] Brown CS, Cassidy NJ, Egan SS, Griffiths D. Numerical modelling of deep coaxial borehole heat exchangers in the Cheshire Basin, UK. Comput Geosci 2021;152:104752.

[28] Nikitin A, Farahnak M, Deymi-Dashtebayaz M, Muraveinikov S, Nikitina V, Nazeri R. Effect of ice thickness and snow cover depth on performance optimization of ground source heat pump based on the energy, exergy, economic and environmental analysis. Renew Energy 2022;185:1301–17.

[29] Schlosser F, Jesper M, Vogelsang J, Walmsley T, Arpagaus C, Hesselbach J. Large-scale heat pumps: Applications, performance, economic feasibility and industrial integration. Renew Sustain Energy Rev 2020;133:110219.

[30] Jesper M, Schlosser F, Pag F, Walmsley TG, Schmitt B, Vajen K. Large-scale heat pumps: Uptake and performance modelling of market-available devices. Renew Sustain Energy Rev 2021;137:110646.

[31] Chen S, Witte F, Kolditz O, Shao H. Shifted thermal extraction rates in large borehole heat exchanger array–A numerical experiment. Appl Therm Eng 2020;167:114750.

[32] Chen S, Cai W, Witte F, Wang X, Wang F, Kolditz O, Shao H. Long-term thermal imbalance in large borehole heat exchangers array–A numerical study based on the Leicester project. Energy Build 2021;231:110518.

[33] Witte F, Tuschy I. TESPy: Thermal engineering systems in python. J Open Sour Softw 2020;5(49):2178.

[34] Chen C, Witte F, Tuschy I, Kolditz O, Shao H. Parametric optimization and comparative study of an organic Rankine cycle power plant for two-phase geothermal sources. Energy 2022;252:123910.

[35] Pfeiffer WT, Witte F, Tuschy I, Bauer S. Coupled power plant and geostorage simulations of porous media compressed air energy storage (PM-CAES). Energy Convers Manage 2021;249:114849. http://dx.doi.org/10.1016/j.enconman.2021.114849.

[36] Gasanzade F, Witte F, Tuschy I, Bauer S. Integration of geological compressed air energy storage into future energy supply systems dominated by renewable power sources. Energy Convers Manage 2023;277:116643.

[37] Dong S, Yu Y, Wang H, Yao Y, Ni L. An economic-energetic-environmental evaluation algorithm for hybrid mid-depth geothermal heating system. Energy 2023;128903.

[38] Bae S, Nam Y. Economic and environmental analysis of ground source heat pump system according to operation methods. Geothermics 2022;101:102373.

[39] Luo J, Rohn J, Bayer M, Priess A, Xiang W. Analysis on performance of borehole heat exchanger in a layered subsurface. Appl Energy 2014;123:55–65.

[40] Brown CS, Kolo I, Banks D, Falcone G. Comparison of the thermal and hydraulic performance of single U-tube, double U-tube and coaxial medium-to-deep borehole heat exchangers. Geothermics 2024;117:102888.

[41] Hu X, Banks J, Guo Y, Liu WV. Retrofitting abandoned petroleum wells as doublet deep borehole heat exchangers for geothermal energy production—a numerical investigation. Renew Energy 2021;176:115–34.

[42] Kolo I, Brown CS, Nibbs W, Cai W, Falcone G, Nagel T, Chen C. A comprehensive review of deep borehole heat exchangers (DBHEs): subsurface modelling studies and applications. Geotherm Energy 2024;12(1):19.

[43] Kolditz O, Bauer S, Bilke L, Böttcher N, Delfs J-O, Fischer T, Görke UJ, Kalbacher T, Kosakowski G, McDermott C, et al. OpenGeoSys: an open-source initiative for numerical simulation of thermo-hydro-mechanical/chemical (THM/C) processes in porous media. Environ Earth Sci 2012;67(2):589–99.

[44] Bilke L, Flemisch B, Kalbacher T, Kolditz O, Helmig R, Nagel T. Development of open-source porous media simulators: Principles and experiences. Transp Porous Media 2019;130(1):337–61. http://dx.doi.org/10.1007/s11242-019-01310-1.

[45] Jakob W, Rhinelander J, Moldovan D. Pybind11–seamless operability between C++ 11 and Python. 2017, URL: https://github.com/pybind/pybind11.

[46] Diersch H-J, Bauer D, Heidemann W, Rühaak W, Schätzl P. Finite element modeling of borehole heat exchanger systems: Part 1. Fundamentals. Comput Geosci 2011;37(8):1122–35. http://dx.doi.org/10.1016/j.cageo.2010.08.003.

[47] Chen C. Investigation on the heat extraction performance of deep closed-loop borehole heat exchanger system for building heating (Ph.D. thesis), Technische Universität Dresden; 2022.

[48] Bell IH, Wronski J, Quoilin S, Lemort V. Pure and pseudo-pure fluid thermophysical property evaluation and the open-source thermophysical property library CoolProp. Ind Eng Chem Res 2014;53(6):2498–508. http://dx.doi.org/10.1021/ie4033999.

[49] Witte F. Thermal Engineering Systems in Python. 2024, https://tespy.readthedocs.io/. [Accessed 01 January 2024].

[50] Cai W, Wang F, Zhang Y, Jiang J, Wang Q, Shao H, Kolditz O, Nagel T, Chen C. Field test and long-term heat extraction performance evaluation of the deep U-type borehole heat exchanger system. Renewable Energy 2024;122171. http://dx.doi.org/10.1016/j.renene.2024.122171.

[51] Triebs MS, Papadis E, Cramer H, Tsatsaronis G. Landscape of district heating systems in Germany – Status quo and categorization. Energy Convers Manage: X 2021;9:100068. http://dx.doi.org/10.1016/j.ecmx.2020.100068.

[52] Triebs MS, Tsatsaronis G. From heat demand to heat supply: How to obtain more accurate feed-in time series for district heating systems. Appl Energy 2022;311:118571. http://dx.doi.org/10.1016/j.apenergy.2022.118571, URL https://www.sciencedirect.com/science/article/pii/S0306261922000551.

[53] Wagner W, Pruß A. The IAPWS formulation 1995 for the thermodynamic properties of ordinary water substance for general and scientific use. J Phys Chem Ref Data 2002;31(2):387–535. http://dx.doi.org/10.1063/1.1461829.

[54] Chen C, Binder M, Oppelt L, Hu Y, Engelmann C, Arab A, Xu W, Scheytt T, Nagel T. Modeling of heat and solute transport in a fracture-matrix mine thermal energy storage system and energy storage performance evaluation. J Hydrol 2024;636:131335.

[55] Deng J, Peng C, Su Y, Qiang W, Cai W, Wei Q. Research on the heat storage characteristic of deep borehole heat exchangers under intermittent operation mode: Simulation analysis and comparative study. Energy 2023;282:128938.

[56] Fu H, Fang L, Yu M, Cui P, Zhang W, Mao Y, Zhuang Z, Fang Z. Influence and economic analysis of heat storage in the non-heating season on the heat extraction capacity of mid-deep borehole heat exchangers. Energy Build 2023;278:112619.

[57] Zeng C, Yuan Y, Haghighat F, Panchabikesan K, Cao X, Yang L, Leng Z. Thermo-economic analysis of geothermal heat pump system integrated with multi-modular water-phase change material tanks for underground space cooling applications. J Energy Storage 2022;45:103726.

[58] Bär K, Rühaak W, Welsch B, Schulte D, Homuth S, Sass I. Seasonal high temperature heat storage with medium deep borehole heat exchangers. Energy Procedia 2015;76:351–60.